

Physiological-Model-Based Neural Network for Heart Rate Estimation during Daily Physical Activities

Yaowen Zhang¹ and Libera Fresiello², Peter H. Veltink¹, Dirk W. Donker^{2,3}, Ying Wang¹

¹Dept. of Biomedical Signals and Systems, University of Twente, Enschede, The Netherlands

²Dept. of Cardiovascular and Respiratory Physiology, University of Twente, Enschede, The Netherlands

³University Medical Center Utrecht, Utrecht, The Netherlands

June 11, 2025

Abstract

Heart failure (HF) poses a significant global health challenge, with early detection offering opportunities for improved outcomes. Abnormalities in heart rate (HR), particularly during daily activities, may serve as early indicators of HF risk. However, existing HR monitoring tools for HF detection are limited by their reliability on population-based averages. The estimation of individualized HR serves as a dynamic digital twin, enabling precise tracking of cardiac health biomarkers. Current HR estimation methods—categorized into physiologically-driven and purely data-driven models—struggle with efficiency and interpretability. This study introduces a novel physiological-model-based neural network (PMB-NN) framework for HR estimation based on oxygen uptake ($\dot{V}O_2$) data during daily physical activities. The framework was trained and tested on individual datasets from 12 participants engaged in activities including resting, cycling, and running. By embedding physiological constraints, which were derived from our proposed simplified human movement physiological model (PM), into the neural network (NN) training process, the PMB-NN model adheres to human physiological principles while achieving high estimation accuracy, with a median R^2 score of 0.8 and an RMSE of 8.3 bpm, even in the presence of intermittent data. Comparative statistical analysis demonstrates that the PMB-NN achieves performance on par with the benchmark fully connected neural network (FCNN) model while significantly outperforming traditional physiological model (PM) ($p=0.002$). In addition, our PMB-NN is adept at identifying personalized parameters of the PM, enabling the PM to generate reasonable HR estimation. The proposed framework with a precise $\dot{V}O_2$ estimation system derived from body movements enables the future possibilities of personalized and real-time cardiac monitoring during daily life physical activities, offering the potential to enhance HF risk detection by improving accuracy and physiological plausibility.

Keywords: Cardiac monitoring, Heart rate estimation, Oxygen uptake, Physiological model-based neural network, Interpretable AI

1 Introduction

Heart failure (HF) contributes to an escalating global health problem, affecting over 15 million people in Europe and imposing a significant socio-economic burdens on both patients and healthcare systems [1, 2]. Early detection of HF would offer opportunities for implementing lifestyle changes and early pharmacological treatments with the great potential to slow the progression of the disease and enhance patient outcomes [3]. Alterations in HR patterns can enable healthcare practitioners to detect warning signs of HF through daily monitoring and promptly conduct further investigations for diagnosis. Elevated resting heart rate (HR) and impaired HR recovery after exercise are strong clinical indicators of HF [4, 5, 6]. Additionally, an increasing rate in HR at the onset of exercise is relative to higher cardiovascular mortality, while suppressed peak HR during exercise has been shown to carry significant prognostic value for HF [7]. Given these findings, abnormalities in HR fluctuations are expected to manifest during daily activities in individuals at risk for HF or those with chronic HF, further underscoring the abnormalities’ relevance in continuous monitoring and early detection [8, 9, 10].

However, existing HR monitoring systems provide limited utility in daily practice as they primarily assess cardiac health by comparing detected HR values with population-based averages [11, 12]. These averages generally do not represent individual’s normal HR fluctuations especially during different physical activities in daily life. It is therefore essential to establish a highly representative real-time personalized HR estimation model that can serve as individual’s digital twin to fairly track their cardiac health condition.

Conventionally, HR estimation models consist of a mathematical representation of the cardiovascular circulation and control mechanism response to aerobic exercise with physiology knowledge embedded [13, 14]. These models have been significantly refined to replicate the main circulatory subsystem representations within the body, thereby enabling accurate simulations of cardiovascular responses to aerobic exercise. However, sole mathematical models are designed to tailor the HR estimation to specific postures or activity scenarios, for instance, participants were instructed to keep the supine position [13] or cycling at a constant rate of 60 rpm [15]. Beyond the contextual limitations, these models include numerous cardiovascular parameters whose values are typically tuned according to standard population representative values, while their computational efficiency is limited by the complexity arising from the multiple interacting variables. Accordingly, it is challenging and unfeasible to use these models for timely and personalized HR estimation during daily activities.

Data-driven approaches offer high efficiency and accuracy in HR estimation and have been extensively employed, particularly using data acquired from wearable devices in daily life scenarios [16]. Neural network (NN) based optimization algorithms have been implemented in continuous HR estimation in daily activity scenarios [17, 18], while regression models, such as multiple regression [19, 20], auto-regressive models [21], support vector regression [22], and k-Nearest Neighbors regression [23] have been utilized to investigate the estimation of HR based on various vital signals. However, data-driven approaches still fail to generate physiologically explainable models [24], particularly in the healthcare domain, where data collection requires significant efforts.

To overcome the limitations mentioned beforehand, we hypothesized that a proper combination of the simplified conventional physiology models and the data-driven models can

leverage both the physiological model’s explainability and the data-driven model’s estimation accuracy. Accordingly, in this study, we proposed a simplified physiological model (PM) for estimating HR during daily activities. Building upon this, we introduced a hybrid framework, the physiological-model-based neural network (PMB-NN), for personalized HR estimation. The PMB-NN was inspired by recent emerging Physics-Informed Neural Network technology, which utilizes existing prior physical knowledge in data-driven modeling practice [25, 26, 27]. We further specify our hypotheses as follows:

1. the proposed simplified PM can demonstrate a reasonable capability for estimating HR across various activities;
2. the proposed PMB-NN model can elevate the performance of the sole PM;
3. the proposed PMB-NN model can achieve equivalent performance as the sole data-driven model;
4. the proposed PMB-NN model is capable of identifying physiologically relevant parameters, which are specifically defined and assigned within the context of the model.

2 Methodology

2.1 Dataset and Data Pre-processing

This study was carried out using the WEEE dataset [28], which is a multi-device and multi-modal dataset collected from 17 participants during different physical activities. Individual’s oxygen uptake $\dot{V}O_2$ data collected by $\dot{V}O_2$ Master Analyzer, and heart rate (HR) data collected by the Wahoo Tickr chest strap during physical activities were used for the PMB-NN model’s development.

The included 12 participants aged between 23 and 40 years (median: 27) followed a physical activity protocol which consists of three types of physical activities: resting, cycling and running. During the resting phase, participants were instructed to sit on a chair for a duration of 5 minutes, followed by a subsequent 5-minute period of standing. Subsequently, participants engaged in aerobic activities, which were 10-minute cycling on an indoor stationary bike and 10-minute running on a treadmill. Both cycling and running activities were executed at two distinct intensity levels chosen by the individuals based on their fitness level [28], and each level activity lasted 5 minutes. Five participants’ data were excluded from the WEEE dataset after our data screening according to theoretical physiological responses ($n=3$; $1/3$ of the HR data from participants 07, 10, and 11 are inversely proportional to $\dot{V}O_2$ signals) and data missing ($n=2$; $\dot{V}O_2$ data after standing is missing from participant 14, and $\dot{V}O_2$ data for running is missing from participant 16).

Oxygen uptake and heart rate data were synchronized with the same time scale and both interpolated with the sampling rate of 1Hz in [28]. Given that $\dot{V}O_2$ signals are normally noisy due to large flow variation and motion artifacts especially in high-intensity activities [29], a first-order Savitzky-Golay high-pass filter [30] was applied to remove peak variations and motion artifacts in $\dot{V}O_2$ signals, and a low-pass finite impulse response filter [31] with window size of 10 samples was applied to smoothen both $\dot{V}O_2$ and HR signals, as this size

is optimal for maintaining $\dot{V}O_2$ signal integrity while effectively removing noise. The signals before and after pre-processing are shown in the Appendix A.

2.2 Physiological Model

2.2.1 Conceptual Model

Our proposed conceptual model describes a simplified close-loop heart rate control system responding to physical activity. A block diagram describing the regulatory mechanisms is shown in Figure 1. This model mainly comprises: the cardiovascular system in 3 main compartments (heart mechanics, heart rate and vessels); a feedback pathway that represent the negative control loop of the baroreflex; a metabolic control block that takes into account the intensity of physical activity. This latter is modeled as a primary stimulus that induces changes in the metabolic regulation and autonomic nervous system (ANS). ANS has a direct effect on sympathetic activities affecting the heart and vessels, and on vagal activity affecting the heart rhythm only [13]. Sympathetic activities towards the heart result in cardiac contractility enhancement and increase in heart rhythm to increase cardiac output (CO). Both efferent sympathetic fibers on vessels and metabolic regulation cause total peripheral resistance (TPR) decrease which is essential to guarantee a higher perfusion to the exercising cardiovascular regions [13].

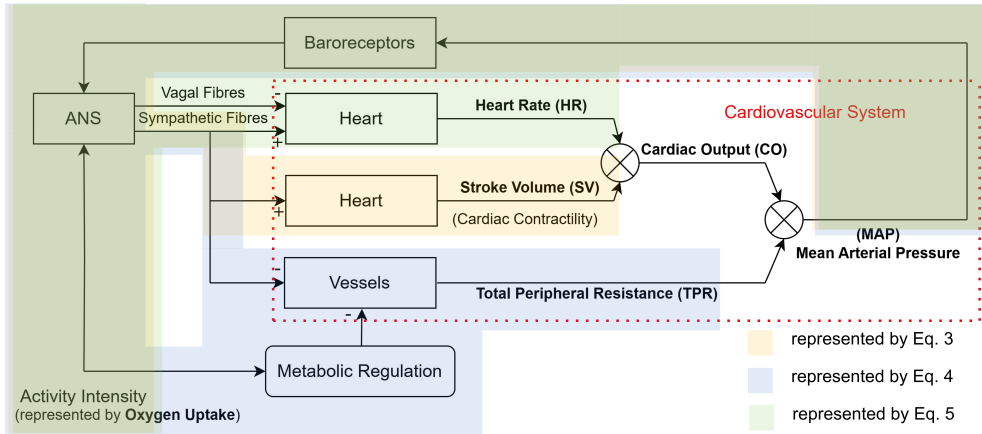


Figure 1: Conceptual model of regulation of heart rate response to physical activity intensity. The bolded variables correspond to those included in the mathematical model outlined later in 2.2.2. The regulatory mechanisms, indicated by distinct colors in the figure, are detailed in equations 3 to 5.

2.2.2 Mathematical Model

In this study, we proposed a simplified physiological model (referred as PM throughout the manuscript) to estimate HR and incorporate physiological constraint in PMB-NN structure. We treated oxygen uptake ($\dot{V}O_2$; unit: L/min) and heart rate (HR; bpm) as our model input and output, respectively. The $\dot{V}O_2$ was chosen as the model input because it is a well-known variable to indicate energy expenditure that quantifies physical activity intensity [32]. The

physiologically dynamic relationship between $\dot{V}O_2$ and HR change, which is illustrated in the conceptual model (Figure 1), was simplified based on the following two assumptions and the classic circulation model from [13] for various freely physical activity occasions to focus on the key physiological mechanisms and reduce computational load for potential daily monitoring applications. Our two assumptions are listed below:

1. we assumed that the relationship between stroke volume (SV) and $\dot{V}O_2$, and between TPR and $\dot{V}O_2$ can be described as a logarithmic function, respectively, based on a previous study about the cardiovascular response of healthy adults during rest and graded intensity of cycling exercises [33].
2. we assumed that the HR is linearly related to the mean arterial pressure (MAP) changes during different activity intensities based on the approximately linear relationship between the change of HR and the change of MAP from rest to exercise observed in [13].

Explanation and validation procedure of the assumption is provided in the Appendix B and C.

Accordingly, we mathematically described the simplified model as the following four algebraic equations: Eq.1-4 and a differential equation (DE): Eq.5.

The cardiovascular system component illustrated in Figure 1 was represented by the Eq.1-2. Cardiac output (CO) is the total volume of blood pumped by the ventricle per minute and defined as the product of the heart rate and the stroke volume, which is,

$$CO(t) = HR(t) \cdot SV(t) \quad (1)$$

where $CO(t)$, $HR(t)$ and $SV(t)$ denote the time series of cardiac output, heart rate and stroke volume with the unit of L/min, beats/min, and L/beat, respectively. Mean arterial pressure (MAP) is the average arterial pressure throughout one cardiac cycle including the systole, and diastole. The relationship between the total peripheral resistance (TPR) and MAP was described by Eq.2:

$$MAP(t) = CO(t) \cdot TPR(t) \quad (2)$$

where $MAP(t)$ and $TPR(t)$ denote the time series of mean arterial blood pressure with the unit of mmHg and total peripheral resistance with the unit of mmHg/L/min, respectively.

The logarithm functions to describe the relationship between SV and $\dot{V}O_2$, and between TPR and $\dot{V}O_2$ are described by the Eq.3 and 4, respectively

$$SV(t) = \lambda_1 \cdot \ln \dot{V}O_2(t) + \lambda_2 \quad (3)$$

where λ_1 and λ_2 , both with the unit of L/min, denote the unknown slope and bias parameters of the logarithmic function from $\dot{V}O_2$ to SV.

$$TPR(t) = \lambda_3 \cdot \ln \dot{V}O_2(t) + \lambda_4 \quad (4)$$

where λ_3 and λ_4 , both with the unit of mmHg/L/min, denote the unknown slope and bias parameters of the logarithmic function from $\dot{V}O_2$ to TPR. the Appendix B provided detailed explanation and validation procedure of the assumption.

The linear relationship to represent the relationship between change of HR and change of MAP is described by the Eq.5.

$$\frac{\partial HR(t)}{\partial t} = \lambda_5 \cdot \frac{\partial MAP(t)}{\partial t} + \lambda_6 \quad (5)$$

where λ_5 and λ_6 , with the unit of bpm/mmHg and bpm/min, respectively, denote the slope and bias of the linear function between change of MAP and change of HR, respectively.

In summary, we solved the system of equations (Eq.1-5) by substitution and derived the Eq.6.

$$F = \frac{\partial HR(t)}{\partial t} - \lambda_6 - \lambda_5 \cdot \frac{\partial \left(HR(t) \cdot (\lambda_1 \log(\dot{V}O_2(t)) + \lambda_2) \cdot (\lambda_3 \log(\dot{V}O_2(t)) + \lambda_4) \right)}{\partial t} \quad (6)$$

A general first order differential equation form can replace Eq.6:

$$HR_t = f(HR, \dot{V}O_2, t, \lambda_s) \quad (7)$$

where HR_t is the time derivative of HR and f is the function of time derivative of product that includes HR and logarithmic of $\dot{V}O_2$ in Eq.6. λ_s represent λ_1 to λ_6 in Eq.6. The data-fitted initial value and physiologically explainable ranges of λ_s are defined based on normal healthy values in cardiovascular hemodynamics for the system identification and presented in Table 1, with detailed explanations available in the Appendix B and C.

λ_s	Initial value	Explainable range	Unit
λ_1	0.02	(0.01, 0.03)	L/min
λ_2	0.1	(0.06, 0.15)	L/min
λ_3	-5.3	(-6, -2)	mmHg/L/min
λ_4	10.5	(7, 20)	mmHg/L/min
λ_5	0.44	(0.1, 0.6)	bpm/mmHg
λ_6	0.3	(-0.5, 0.5)	bpm/min

Table 1: Initial values and ranges for λ_s

The performance of the sole physiological model was evaluated through fitting the mathematical formulation in Eq.6, where the λ_s were optimized via the limited-memory Broyden–Fletcher–Goldfarb–Shanno (LM-BFGS) algorithm on the training set and subsequently validated on the testing set for each individual subject.

2.3 PMB-NN Architecture and Algorithms

The structure of our PMB-NN framework is shown in Figure 2. The PMB-NN was trained to respect both the measured HR training data fitting and the cardiac physiology mechanisms, which are described by our mathematical model in 2.2.2. Notably, the PMB-NN is built on the architecture of a fully connected neural network (FCNN), with an additional loss term for

physiologically explainable estimation. The data fitting aspect was introduced to the PMB-NN framework via the data fitting term defined by a L_2 loss (cost) function (L_{data}) in the Eq.8, and the physiology mechanism aspect was introduced via the physiological constraint term defined by a L_2 loss (cost) function (L_{DE}) in the Eq.9.

$$L_{data} = \frac{1}{N} \sum_{i=1}^N (HR_{data,i} - HR_{pred,i})^2 \quad (8)$$

$$L_{DE} = \frac{1}{N} \sum_{i=1}^N (HR_{t,pred,i} - f(HR_{pred,i}, VO_{2,pred,i}, t_i, \lambda))^2 \quad (9)$$

where N is the number of data points, while t_i is the time of each data point. $HR_{data,i}$ and $\dot{VO}_{2,data,i}$ denote the measured HR and \dot{VO}_2 value at t_i , respectively. $HR_{pred,i}$ and $HR_{t,pred,i}$ denote the estimated HR value and its time derivative at the same time of t_i . The unknown parameters in the mathematical model (λ_1 to λ_6) were assigned initial values and constrained within the ranges specified in Table 1.

Ultimately, we define the total loss L_{tot} as:

$$L_{tot} = L_{data} + L_{DE} \quad (10)$$

We assign a weight of 1 to L_{data} and 10^5 to L_{DE} , ensuring that both loss terms operate on the same order of magnitude, thereby contributing equally to the optimization process of the PMB-NN framework.

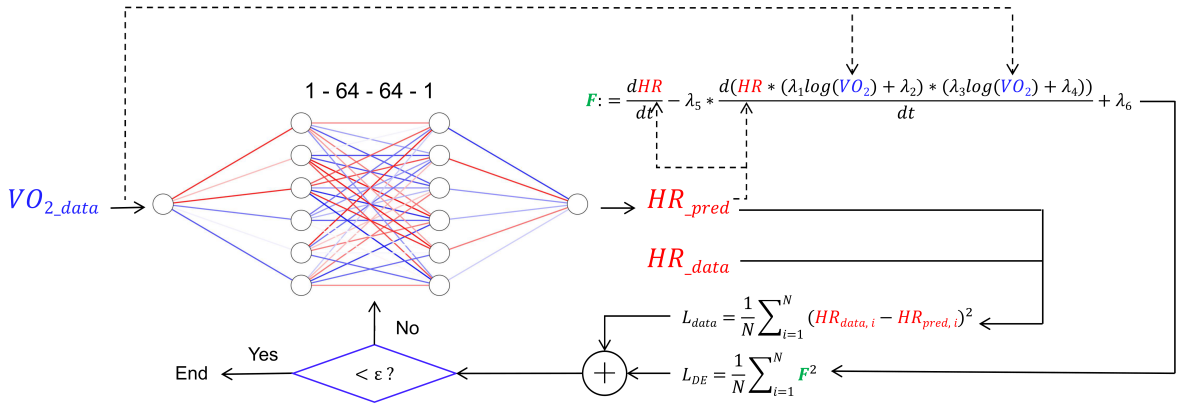


Figure 2: Schematic of PMB-NN framework in this study. After initialization of the neural network structure and parameters in the physiological model, predicted HR (HR_{pred}) values were obtained from the inputs \dot{VO}_2 data by a forward pass multilayer perceptron (MLP). The HR_{pred} values was substituted to both data fitting term (L_{data}) and the physiology constraint loss term (L_{DE}) afterwards. The sum of the two terms (L_{tot}) was used for random search to update both the physiological model parameters in Eq.6 and the hyperparameters in MLP.

Algorithm 1 gives a detailed flow illustration of the PMB-NN training algorithm.

Algorithm 1: PMB-NN Training Algorithm

Require: Training set containing $\dot{V}O_2$ and HR

- 1: **Initialization:**
 - 2: Set neural network layer structure as 1-64-64-1
 - 3: Set activation function as *Tanh*
 - 4: Set the unknown parameters (λs) in the mathematical model to initial values and constrain within the specific ranges
 - 5: Set optimizer as RMSprop and learning rate as 0.01
 - 6: **Loss terms definition:**
 - 7: Define L_{data} according to equation 8
 - 8: Define L_{DE} according to equation 9
 - 9: Define $L_{tot} = L_{data} + L_{DE} \cdot 10^5$
 - 10: **for** each epoch **do**
 - 11: **Training Phase:**
 - 12: Perform forward pass
 - 13: Compute training loss (L_{tot})
 - 14: Perform back propagation and update model parameters including hidden parameters and λs
 - 15: Record training loss and λs
 - 16: **if** $L_{tot} < \epsilon$ **then**
 - 17: **return** Hidden parameters and λs for testing phase
 - 18: **else**
 - 19: Repeat training for up to 5000 iterations
 - 20: **return** Hidden parameters and λs for testing phase
 - 21: **end if**
 - 22: **end for**
-

The PMB-NN framework was trained on a workstation equipped with 12th Gen Intel(R) Core(TM) i7-12700H CPU. Deep learning framework Pytorch 2.1.0 in Python 3.9.13 was fully applied in establishing our algorithm. A fully-connected neural network structure was initialized. Two hidden layers and 64 neurons setting in each layer allowed for extraction and representation of complex features within the data and mitigated the risk of overfitting. Tangent activation function (*Tanh*) helped in learning nonlinear relationships between $\dot{V}O_2$ and HR therefore guaranteed the model’s fitting capability. Setting the optimizer as Root Mean Squared Propagation (RMSprop) helped in maintaining a balance between speed and stability of the training process. The learning rate was chosen as 0.01 to empirically balance convergence speed and stability, ensuring efficient training of the model.

The PMB-NN framework was optimized by minimizing the loss function in Eq.10, iteratively updating both the neural network weights and the unknown parameters. In each epoch, the model performed a forward pass, followed by backpropagation to calculate gradients, which were used in the weight update process via gradient descent. To ensure that physical constraints on model parameters were respected, the lambda parameters were initialized with values based on physiological knowledge and were updated during training. These parameters were mapped to a physically explainable range using a sigmoid function, preventing them from exceeding defined upper and lower boundaries. The training process was stopped once the total loss dropped below an empirically set threshold of 10 bpm or after 5000 epochs, whichever came first, revealing that the model had converged and further iterations would not significantly improve performance.

2.4 Dataset Synthesization

Based on the original dataset, we synthesized a new dataset that can capture the large activity variety nature of physical activities in daily living because the original dataset was collected with a single non-repetitive prototype: resting-cycling-running. The dataset synthesization process is illustrated in the Figure 3. In detail, the original data set for each participant was divided into three segments according to the activity types: resting, cycling and running. Then each segment was divided into its 80% and 20%. The 80% of the three segments were merged into the training set, while the rest 20% segments were merged into the testing set.

2.5 Model Evaluation

We tested our four hypotheses in the following evaluation approaches:

1. To test the first hypothesis regarding the simplified PM model’s capacity for HR estimation, we examined the performance of the PM model.
2. To test the second hypothesis, which posits that the PMB-NN outperforms the PM model, we compared the paired performance results of the PMB-NN and PM models.
3. To test the third hypothesis, which suggests that PMB-NN provides comparable estimation performance to the benchmark model, we conducted a paired comparison between the PMB-NN and FCNN models.

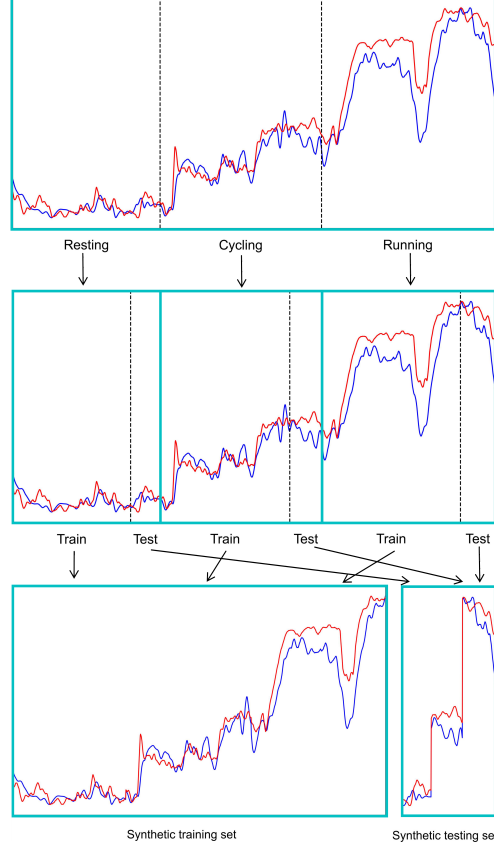


Figure 3: Dataset synthesization illustration. The first row figure indicates the processed dataset including three activity types. The second row figures indicate the splitted segments according to activity types. Each segment was divided as training and testing set with the ratio of 8:2. The third row indicate the synthetic training set and synthetic testing set from splicing all the training and testing segments, respectively.

4. To test the fourth hypothesis regarding PMB-NN's ability to identify physiologically explainable parameters, the personalized lambda values identified by PMB-NN were substituted into the PM model. This method, named as 'PMB-NN-R', resulted in the output, referred to as 'reconstructed HR'. We then compared the paired performances of the PMB-NN-R and PM models to validate the effectiveness of the lambda values identified by PMB-NN.

PMB-NN, FCNN and PM were trained and tested on the same training and testing sets described in 2.4, respectively. We evaluated each model's performance through evaluation metrics as follows:

1. The coefficient of determination is denoted by R^2 and indicates the proportion of the variance in measured HR that can be explained by the estimated HR. The R^2 is defined in the Eq.11 where HR_i and \hat{HR}_i represent reference value and estimated value of HR, respectively. \bar{HR} in the denominator represents the average value of HR_i and n denote the number of data points.

2. The root mean square error (RMSE) represents the standard deviation of the residuals and measures the average magnitude of the errors between the estimated HR and the reference HR. RMSE is defined in Eq.12 where HR_i , $\hat{H}R_i$ and n have the same definitions as mentioned in Eq.12.

$$R^2 = 1 - \frac{\sum_{i=1}^n (HR_i - \hat{H}R_i)^2}{\sum_{i=1}^n (HR_i - \bar{H}R)^2} \quad (11)$$

$$RMSE = \sqrt{\frac{1}{n} \sum_{i=1}^n (HR_i - \hat{H}R_i)^2} \quad (12)$$

Median, maximum and minimum values of the above evaluation metrics and the computation time were also chosen to evaluate the model’s overall performance. The median values were chosen to guarantee the robustness to outliers given the small sample size (data from 12 participants). The maximum and minimum values were chosen to assess the range of model performance across different conditions. Boxplots were used to visually represent the distribution of the evaluation metrics, including the median, maximum, and minimum values, as well as the spread and potential outliers in the data. This provides a clear overview of the variability and robustness of the model’s performance across participants.

The Wilcoxon signed-rank tests [34] were performed on each pairwise comparisons between PMB-NN and the respective models (N pairs for N participants). A p-value from one-tailed comparison less than or equal to the significance level of 0.05 was treated as statistically significant difference. Cohen’s d was calculated on each same pairwise comparisons to quantify the effect size, with values of 0.2, 0.5, and 0.8 representing small, medium, and large effects, respectively.

3 Results

The overall estimation performance of the PM, PMB-NN and FCNN models were summarized in the following. Both PMB-NN and FCNN reached an appropriate estimation accuracy respectively with R^2 of 0.8 (-0.95, 0.98) and 0.83 (-0.49, 0.98), RMSE of 8.29 (4.88, 18.08) bpms and 8.6 (3.88, 16.78) bpms, while the PM model yielded a relatively lower R^2 of 0.57 (-1.74, 0.95), RMSE of 16.84 (7.8, 36.3) bpms.

The performance of PMB-NN, FCNN, and PM on individual participants is given in the Table 2, the Appendix D. The Wilcoxon signed-rank test revealed that PMB-NN provided significant improved accuracy comparing with PM reflecting in both R^2 ($p=0.002$, $d=-0.669$) and RMSE ($p=0.002$, $d=1.178$), meanwhile reached similar accuracy comparing with FCNN reflected as R^2 ($p=0.26$, $d=0.033$) and RMSE ($p=0.064$, $d=-0.118$). Figure 4 provided the performance summary of both PMB-NN, FCNN, and PM and comparison by listing each evaluation metric in Table 2. A detailed statistical comparison of the three models, evaluated across distinct activity types, is presented in the Appendix E. Activity-specific performance revealed that PMB-NN outperformed PM in cycling (RMSE: $p=0.034$, $d=0.686$). No significant differences were found between PMB-NN and FCNN across all activities.

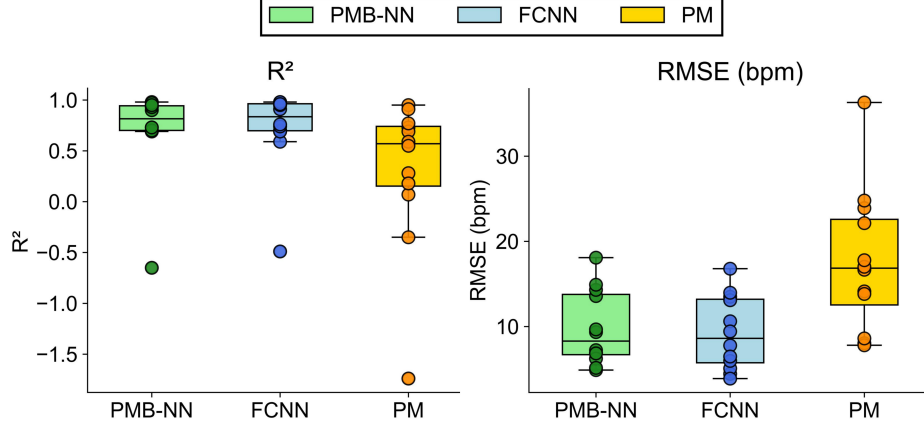


Figure 4: Performance comparison between PMB-NN, FCNN frameworks and PM in HR estimation tasks using box plot. The subplots show the performance of each model across two evaluation metrics: R^2 and RMSE (bpm). In each subplot, the box plot displays the distribution of each metric, with the middle line indicating the median, the box representing the interquartile range (IQR), and the whiskers extending to 1.5 times the IQR or the minimum/maximum value within this range. Individual points outside the whiskers are considered outliers. Green represents the PMB-NN framework, blue represents the FCNN framework, while yellow represents the PM framework.

We presented the PMB-NN, FCNN, and PM results of two participants as visualization examples in Figure 5. As shown in Figure 5a, all three models demonstrated good agreement with the real values during the resting and cycling phase, while PMB-NN and FCNN exhibited relatively lower errors than PM in the running phases, while in Figure 5b, PM exhibited better HR alignment during running phase.

Table 3 in the Appendix E presents the PMB-NN-identified personalized λ values and their corresponding reconstruction (PMB-NN-R) performance metrics, and Table 4 in the Appendix E presents the PM identified λ values. The results indicate that PMB-NN offers greater flexibility and variability compared to PM. While PM maintains a more consistent set of lambda values across participants, PMB-NN shows a broader range of values. There was no significant performance difference between PMB-NN-R (R^2 : 0.60 (-0.27, 0.93); RMSE: 14.41 (7.56, 29.02)) and PM estimation in Table 2 (comparison: R^2 : $p=0.424$, $d=0.344$; RMSE: $p=0.470$, $d=-0.261$).

4 Discussion

This study proposes a physiological model-based neural network structure for heart rate estimation from oxygen uptake signal. The primary contribution of this work lies in the successful integration of physiological principles into a data-driven neural network, which not only enhances the interpretability of the model but also achieves excellent estimation accuracy. The results of this study validate our initial hypotheses. Firstly, the simplified PM is able to demonstrate a reasonable capability in HR estimation. Next, the PMB-NN model significantly outperforms the conventional physiological model meanwhile achieves equivalent

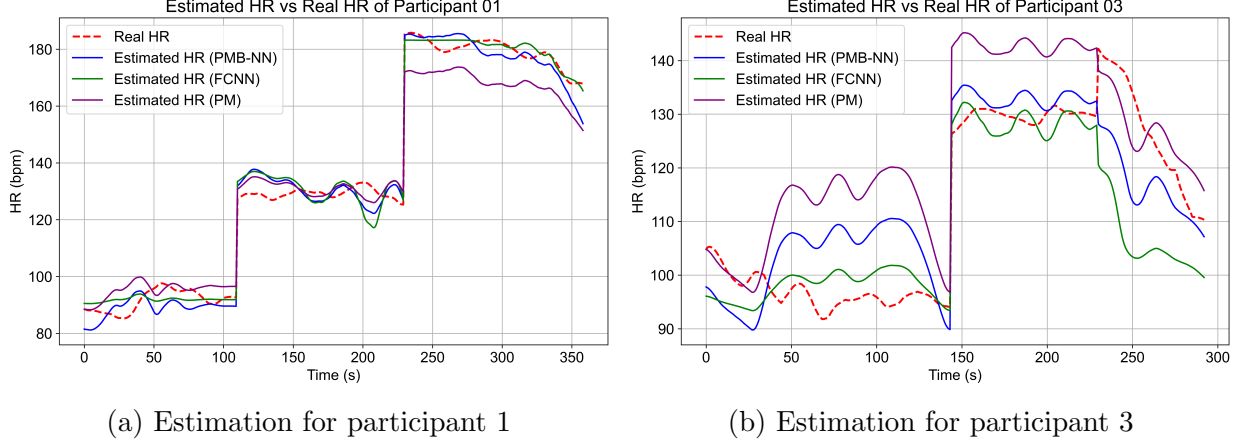


Figure 5: Three models’ HR estimation results of participant 1 and 3. 5a: PMB-NN, FCNN and PM estimated HR comparing with real HR of participant 1. 5b: PMB-NN, FCNN and PM estimated HR comparing with real HR of participant 3. The red dash curve in each plot represents the measured HR values, while the blue, green and purple solid curves represent the PMB-NN, FCNN and PM estimated HR values, respectively.

performance to the benchmark fully connected neural network model. With an overall R^2 of 0.8 and RMSE of 8.29 bpm, the PMB-NN framework demonstrated excellent accuracy ($R^2 \geq 0.75$) [35] in HR estimation. Finally, the PMB-NN is capable in physiologically relevant parameter identification. Deeper exploration of general performance and certain nuanced aspects of individual performance were discussed to understand the limitations, perspective of further development and potential applications of this model.

We observe noticeable performance improvement of PMB-NN compared with PM in Table 2. The superior performance of PMB-NN over PM can be attributed to its hybrid modelling architecture, which couples a fully connected neural network (FCNN) with an explicit physiological loss term. This design allows PMB-NN to overcome the limitations of traditional parametric models by capturing complex, non-linear relationships. The FCNN component allows the model to flexibly approximate a broad range of individual-specific mappings, while the physiological loss term introduces inductive bias grounded in domain knowledge, constraining the solution space toward physiologically explainable behaviours. This dual mechanism enhances both expressivity and interpretability: the network can fit participant-specific data patterns with high fidelity, while the physiological constraint ensures model estimations remain consistent with known physiological principles. Importantly, this synergy enables PMB-NN to generalise better across heterogeneous populations and varying conditions, ultimately yielding superior predictive accuracy and robustness.

The PMB-NN achieves performance comparable to the FCNN in Table 2, by combining the expressive power of neural networks with physiological constraints that guide estimations toward biologically explainable solutions. This integration enables the model to capture individual-specific nonlinear patterns while avoiding overfitting, thus maintaining accuracy on par with the benchmark. Slight differences in R^2 (≥ 0.04) are observed for 4 out of 12 participants, based on pairwise estimation plots and the corresponding metrics in Table 1. These discrepancies may arise from the increased optimization complexity introduced by the physi-

ological constraints. Analysis of training loss curves revealed that, compared to the relatively stable data loss, the physiological loss exhibited substantial fluctuations, indicating that the model struggled to consistently satisfy the differential equation constraint. This reflects an inherent trade-off between minimizing estimation error and enforcing physiological plausibility. Moreover, the limited dataset and invariant structure may have further restricted model performance. To create sufficient training input, we segmented and concatenated the data into shorter windows, a process that likely introduced noise and disrupted temporal continuity of physiological signals. From the interpretable AI perspective, the model’s reliance on physiological constraints introduces a layer of transparency by ensuring that the estimated parameters adhere to known biological principles. This provides valuable insight into how the model’s internal representations align with real-world physiological processes, which makes it more interpretable and fostering trust in the model’s outputs. Future work could collect more diverse and continuous datasets, or adopt augmentation techniques that preserve physiological structure. These may enhance model generalizability across different exercise types and participants.

The PMB-NN demonstrates several advantages over the traditional PM approach in parameter identification. PMB-NN is able to successfully identify individualized λ values across participants. Unlike PM, where many parameter estimates clustered near the boundaries of the predefined search space, the PMB-NN produces a more diverse and physiologically explainable distribution of parameter values. This suggests that the data-driven learning mechanism in PMB-NN allowed for better adaptation to participant-specific features, avoiding the boundary effects that are often observed in optimization-based fitting procedures under rigid constraints. Moreover, PMB-NN achieve reconstruction accuracy comparable to PM, as shown in Table 3. This indicates that the model preserved the predictive strength of the original system while enabling more flexible and individualized parameter estimation. The physiological constraint, enforced through a differential equation-based loss term, likely contributed to the identifiability and realism of the learned parameters without compromising estimation quality. Among the performance metrics of PMB-NN-R, we observe a notable underperformance in participant 6, where the R^2 value was 0.04, compared to 0.69 for the PM model, as shown in Table 2. Upon further investigation of the estimation curves for both models, presented in the Appendix G, we speculate that the physiological constraints introduced by the PMB-NN model may have caused excessive misalignment for participant 6. The larger discrepancy could be due to the model’s difficulty in accurately learning and generalizing the parameter values, particularly with limited data or the complexity of individual-specific cardiovascular dynamics. Also, this observation highlight the model’s sensitivity to variations. Further tuning of the parameters or adjusting of the model could potentially address these discrepancies and improve the performance of PMB-NN-R in such cases.

Our findings also highlight the successful construction of a simplified physiological model (PM) that captures key individual-specific parameters using a compact set of interpretable variables. This model, grounded in domain-informed assumptions and analytically tractable structure, demonstrates the feasibility of deriving physiologically meaningful insights from limited observational data. Its clear parameter formulation offers transparency and potential for exercise physiological interpretability, which make it a useful foundation for applications where model simplicity, interpretability, and low computational cost are essential. Despite

these advantages, the PM framework has limitations. As a model with only one state, it is inherently restricted in its ability to capture dynamic or time-varying physiological processes and to cover the variability that is seen in the data, which are often critical for understanding real-world behaviours such as adaptation, fatigue, or recovery. Additionally, the model’s reliance on pre-defined functional forms and bounded parameter spaces can lead to convergence toward edge solutions, as observed in several participants. Future work could enhance the model by extending it into a time-aware or state-space formulation to capture dynamic cardiovascular transitions. Incorporating hierarchical or Bayesian frameworks may also help quantify uncertainty in parameter estimation while preserving interpretability.

In the PM, parameters λ_1 - λ_6 carries distinct physiological implications. λ_1 and λ_2 govern the logarithmic relationship between SV and $\dot{V}O_2$, where λ_1 may reflect the dynamic enhancement of myocardial contractility during exercise, while λ_2 could represent baseline SV at rest. Similarly, λ_3 and λ_4 , associated with TPR and $\dot{V}O_2$, likely characterize vascular adaptability to metabolic demands. λ_3 indicates the rate of TPR reduction with increasing exercise intensity, and λ_4 reflects baseline vascular tone. λ_5 and λ_6 link HR and MAP changes, may map ANS regulation efficiency, with λ_5 representing sympathetic responsiveness to blood pressure fluctuations and λ_6 potentially denoting parasympathetic baseline inhibition. The individualized variability in these parameters (e.g., broader λ ranges in PMB-NN vs. PM in the Appendix E) quantifies distinct physiological regulatory traits. For example, healthy young adults might exhibit higher λ_1 and λ_6 which indicates robust cardiovascular compensation, whereas elderly individuals may show reduced λ_3 (impaired vascular resistance modulation), reduced λ_2 (lower resting SV) and elevated λ_4 (higher vascular resistance). In cardiovascular disease populations, abnormally low λ_5 could reflect autonomic dysfunction, while deviations in λ_3/λ_4 might reflect endothelial impairment. Integrating these parameters with interpretable AI frameworks is potential for enhancing personalized predictions and enabling mechanistic insights for clinical applications.

The prevalence of negative R^2 values in the Appendix F underscore the metric’s susceptibility to model misspecification, as it penalizes deviations from an oversimplified constant mean baseline, whereas RMSE retains interpretability by quantifying absolute estimation errors independent of reference models. The integration of p-values and Cohen’s d effect sizes becomes critically instructive in our stratified analyses, where both limited sample size ($n=12$) and truncated data segments per activity synergistically constrain statistical power. While conventional p-values struggle to detect significance in fragmented datasets, as observed in the resting-state comparisons where PMB-NN exhibited a moderate effect ($d=-0.607$) in RMSE but non-significant underperforming p-values ($p=0.064$) comparing with FCNN, effect sizes quantify the magnitude of differences independent of sample variability, unmasking trends obscured by motion-specific data partitioning. For instance, in cycling, PMB-NN’s RMSE advantage to PM achieved both statistical significance ($p=0.034$) and a robust effect ($d=0.686$), whereas in running, yielding negligible effects ($d=0.548$) despite comparable p-values ($p=0.077$). These results suggest that with a larger sample size, the potential performance advantage of PMB-NN over traditional models may become more pronounced, helping to detect more subtle yet important trends that are currently masked by the smaller sample size. This duality underscores that effect sizes contextualize p-values by distinguishing statistical noise from biologically explainable effects, particularly when activity stratification reduces within-group data continuity.

It is noted that the performance of PM and PMB-NN demonstrated a consistent pattern across different participants; both models excelled or underperformed in tandem. This synchronicity implies that the inherent characteristics of individual participants exert a uniform influence on the efficacy of both models. An example of processed data from participant 2 is given in the Appendix H. Upon closer inspection of the processed data for five participants (02, 03, 06, 09 and 15), a shared trend emerged: each exhibits a sudden increase in HR after first 5 minutes, from approximately 60-70 bpm to 90-100 bpm, which can be attributed to a specific physiological response to the "sit-to-stand" stimulus. This stimulus activates the sympathetic nervous system, prompting an immediate rise in HR as the body adjusts to postural change. Following this initial surge, HR gradually decreases to its resting level. However, during this HR adjustment period, $\dot{V}O_2$ remains relatively stable, showing minimal fluctuations. This lack of proportionality between the HR and $\dot{V}O_2$ signals creates a unique challenge for the PMB-NN model, which relies on the assumed relationship (described in the Eq.3, 4 and 5) between these two physiological indicators.

On the other hand, participant 13 demonstrates a relatively low R^2 of -0.65 of PMB-NN. According to the original data set of this participant, $\dot{V}O_2$ showed a rapid increase at the onset of cycling and stays in the same level during the first 5 minutes of cycling. However, HR paradoxically decreased from 130 to 100 bpm within the same period. This response, while unusual, is not entirely unprecedented. In some rare cases, a decrease in HR during the onset of exercise can be attributed to a phenomenon known as exercise-induced bradycardia or a vagal response, where the parasympathetic nervous system remains dominant during initial physical exertion [36]. This could result in a temporary drop in HR despite the increase in $\dot{V}O_2$, as the body adapts to the onset of exercise [36]. Additionally, such responses might also be observed in individuals with high cardiovascular fitness levels, where the heart becomes more efficient in pumping blood and may initially decrease in rate before stabilizing or increasing with prolonged activity [37]. Retaining this participant's data within the model input allows us to better assess the model's generalization capacity across atypical cases. The reliability of the PMB-NN was demonstrated by its strong performance. However, the unsatisfactory performance on participant 13 indicates that the model's ability to generalize across a diverse range of data types still needs improvement.

Several targeted strategies can be pursued to improve its physiological fidelity and generalization capacity. First, to resolve the conflict between mathematical stability and physiological realism caused by loss function imbalance, a dynamic weighting scheme could be implemented to prioritize equation constraints (L_{DE}) during stable physiological states while emphasizing data fidelity (L_{data}) during dynamic activities, thereby mitigating parameter clustering artifacts. Second, architectural improvements such as replacing Tanh activations with Leaky Rectified Linear Unit (Leaky ReLU), could alleviate gradient saturation in autonomic terms (λ_5 - λ_6) and enhance the model's ability to capture abrupt physiological transitions, such as HR spikes during 'sit-to-stand' maneuvers in participants 2 and 3. Additionally, embedding hybrid mechanistic-data layers, such as incorporating the Windkessel model for TPR dynamics as hard constraints, could improve sensitivity to weak monotonicity and stochastic fluctuations then address the oversimplification inherent in the current algebraic-differential framework. Furthermore, leveraging transfer learning from larger cardiovascular datasets could enhance generalization for atypical cases (e.g., participant 13's vagal response) while retaining personalized adaptation through fine-tuning on individual exercise patterns.

Finally, to address the challenges of data scarcity and limited external validation, future work could benefit from the integration of additional non-invasive sensing modalities. In follow-up studies, we plan to collect self-acquired datasets incorporating continuous blood pressure monitoring, which can provide beat-to-beat estimates of SV and TPR (combined with established methods such as Modelflow [38]). These derived measurements will serve as an independent reference for assessing the plausibility and robustness of parameter estimates from the PM, offering a more comprehensive framework for evaluating model validity under varied physiological conditions. Collectively, these refinements aim to harmonize data-driven learning with physiological coherence, enabling robust, individualized HR estimation across diverse populations and advancing the framework’s potential for real-time cardiovascular risk monitoring.

5 Conclusion

In this research, we proposed a physiological model-based neural network (PMB-NN) for heart rate estimation from oxygen uptake signals across various daily activities. The PMB-NN demonstrates promising estimation accuracy equivalent to sole data-driven model and outperforms sole physiological model, due to its integration of physiological principles, which enhances predictive accuracy and model interpretability. Moreover, the simplified physiological model we proposed, along with the individualized parameters identified by PMB-NN, effectively reproduced the dynamics of heart rate responses. This study highlights the potential of combining data-driven methods with physiological insights for personalized health monitoring. Future work may involve refining the physiological model and combining advanced network architectures to build a digital twin for early cardiovascular risk detection in home settings.

A Data preprocessing consequence

An example of data preprocessing consequence is shown in Figure 7.

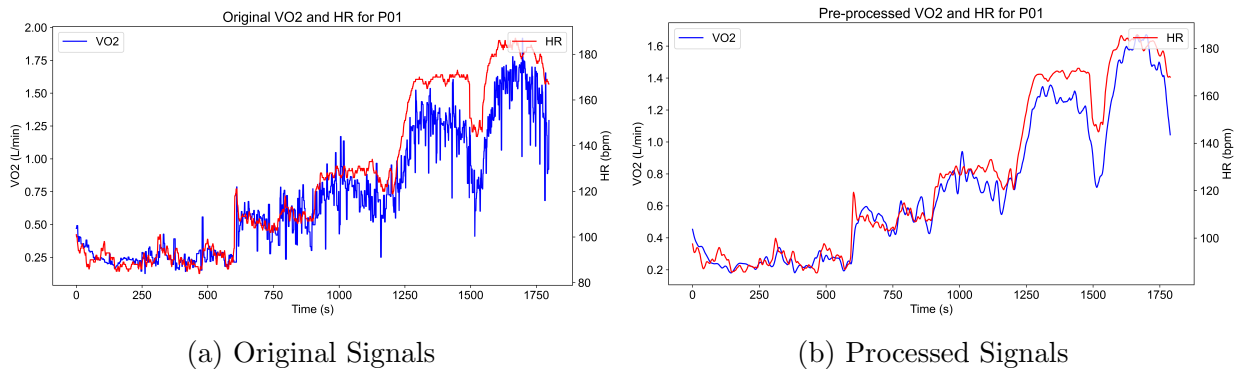


Figure 6: The measured signals and filtered signals of one subject. $\dot{V}O_2$ (blue) and HR (red) signals from measurement (6a) and preprocessed (6b) are plotted in the figure.

B Validation of curve fitting for stroke volume and total peripheral resistance

In figure 7a, we presented the fitted logarithmic curves to the data about the SV and TPR response to $\dot{V}O_2$ in [33], whose SV and TPR data were derived from hemodynamic analysis of HR and ABP recordings. The data had displayed SV and TPR changes within different intensities from resting to submaximal exercise (unit: kpm/min) for 12 healthy participants. We converted the unit from exercise intensity to oxygen uptake according to the formula described in [32]. The R^2 of fit for SV and TPR are 0.98 and 0.99, respectively. Therefore, initial values of 0.02, 0.1, -5.3, and 10.5 were chosen for λ_1 through λ_4 , respectively.

Normal SV values range is 0.057 to 0.144 L/min [39], while TPR typically falls between 8.75 to 20 mmHg/L/min [33, 40, 41]. It is expected that the estimated SV and TPR will lie within these physiologically explainable intervals. Accordingly, we examined the feasible ranges for the unknown parameters λ_1 to λ_4 within the proposed logarithmic functions, guided by the normal ranges of SV, TPR, and $\dot{V}O_2$ reported in [33]. The approximate intervals are: λ_1 (0.01, 0.03), λ_2 (0.06, 0.15), λ_3 (-6, -2), and λ_4 (7, 20). In figure 7b, the explainable ranges of the SV- $\dot{V}O_2$ and TPR- $\dot{V}O_2$ relationships are illustrated.

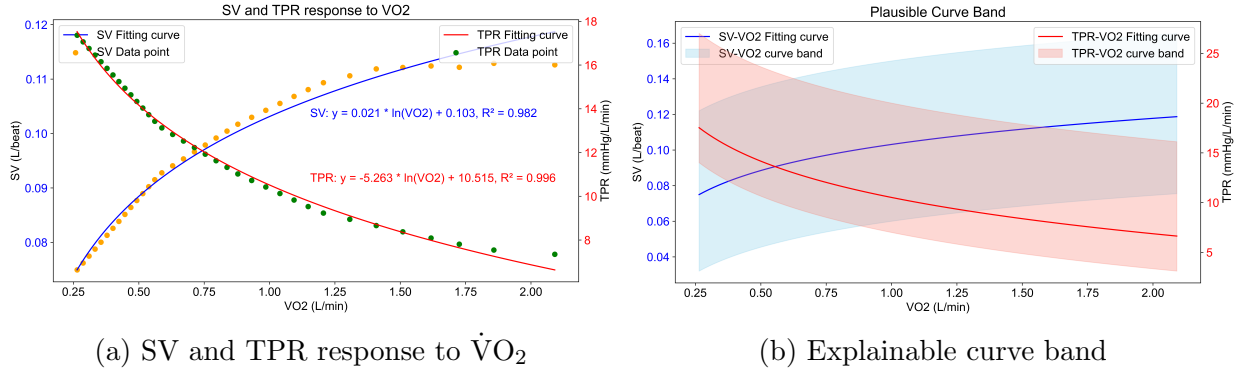


Figure 7: 7a: Logarithmic Regression Curves and Functions for SV and TPR. Orange and green points are SV and TPR data replicated from [33], respectively. Blue and red lines indicate our fitted curves that represent SV and TPR response to $\dot{V}O_2$, respectively. 7b: Possible bands of SV- $\dot{V}O_2$ (in skyblue) and TPR- $\dot{V}O_2$ (in salmon) relationship curve, with ranges as: λ_1 (0.01, 0.03), λ_2 (0.06, 0.15), λ_3 (-6, -2), λ_4 (7, 20) from equation 6.

C Validation of linear relationship between the change of HR and change of MAP

Verification of the linear relationship between ΔHR and ΔMAP was done based on the data in [33]. A continuous 3 minutes' time pattern of HR and MAP wave was simulated with their model in transient phase from rest to moderate exercise. We applied their data to express HR and MAP waveform ($MAP = 1/3 SBP + 2/3 DBP$) shown in figure 8a, resampled at 1 Hz on each waveform (0-180s, 181 points), calculated ΔHR and ΔMAP were

obtained by differentiation from HR and MAP and showed in the hexagonal binning plot of ΔHR and ΔMAP in figure 8b. We disregarded the rapid drop in MAP between 65 and 70 seconds, which was caused by the time delay in the decrease of TPR following the increase in exercise intensity at 1 minute, owing to the omission of time delay dynamics in the simplified $\text{TPR}-\dot{V}\text{O}_2$ model in equation 4.

In Figure 8b, the linear fit effectively captured the relationship between ΔHR and ΔMAP . A total of 167 out of 180 data points (92.78%) fell within the 95% confidence interval, indicating that the majority of the points are closely aligned with the linear regression model. In figure 8c, the explainable ranges of λ_5 and λ_6 in ΔHR - ΔMAP relationship is illustrated. HR changes are generally positively correlated with MAP variations, especially within the regulation mediated by the baroreflex [42]. Based on this prior empirical observation in exercise HR and MAP dynamics accompanied with the fitted values 0.44 and 0.3, we defined the positive range (0.1, 0.6) for λ_5 , while (-0.5, 0.5) for λ_6 which distributed around zero in both positive and negative directions.

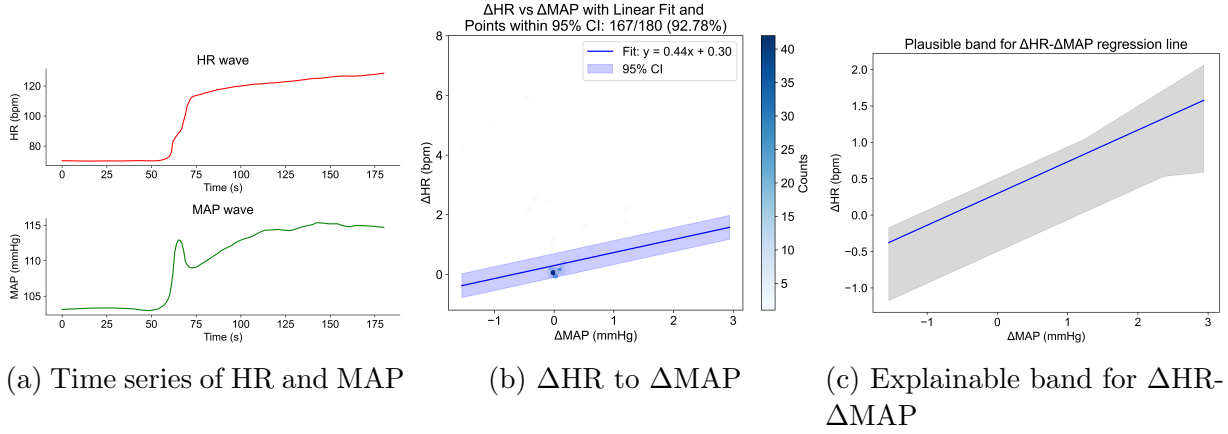


Figure 8: Validation of linear relation between ΔHR and ΔMAP . 8a: Time series of heart rate in red and mean arterial pressure in green. 8b: Linear regression result of ΔHR and ΔMAP . Blue hexagon points with different color depth represent amount and density of ΔMAP and ΔHR . Blue straight line is the linear regression curve for ΔHR and ΔMAP and light blue area is the 95% confidence interval. 8c: Explainable range of the ΔHR - ΔMAP regression line. The blue line represents the current fit, and the shaded area indicates the range of possible lines within the specified parameter bounds. The parameter ranges are (0.1, 0.6) for λ_5 and (-0.5, 0.5) for λ_6 .

D Individualized performance from different models and comparison

Participant	PMB-NN		FCNN		PM	
	R ²	RMSE	R ²	RMSE	R ²	RMSE
01	0.98	4.88	0.98	4.44	0.95	8.03
02	0.70	13.58	0.70	13.49	0.07	23.90
03	0.69	9.34	0.59	10.61	0.28	14.12
04	0.90	9.66	0.91	9.43	0.73	16.67
05	0.94	6.90	0.97	5.07	0.18	24.79
06	0.73	7.23	0.69	7.77	0.69	7.80
08	0.93	6.24	0.95	5.97	0.59	17.01
09	0.70	18.08	0.74	16.78	0.55	22.13
12	0.97	5.15	0.98	3.88	0.91	8.61
13	-0.65	14.30	-0.49	13.09	-1.74	17.78
15	0.73	14.91	0.76	13.97	0.77	13.83
17	0.95	6.84	0.96	6.48	-0.35	36.30
p value	-	-	0.260	0.064	0.002	0.002
d value	-	-	0.033	-0.118	-0.669	1.178

Table 2: Performance metrics for PMB-NN, FCNN, and PM models across participants

E Personally identified values of unknown parameters in mathematical model from both PMB-NN and PM

Participant	PMB-NN						PMB-NN-R	
	λ_1	λ_2	λ_3	λ_4	λ_5	λ_6	R ²	RMSE
01	0.017	0.109	-2.000	19.921	0.404	0.000	0.90	11.62
02	0.012	0.144	-2.000	19.720	0.366	-0.001	0.66	14.31
03	0.015	0.118	-2.000	19.926	0.362	-0.001	0.38	13.09
04	0.020	0.109	-2.000	19.553	0.385	0.002	0.80	14.50
05	0.016	0.125	-2.000	19.786	0.357	0.002	0.70	14.92
06	0.016	0.129	-2.000	19.675	0.349	0.000	0.04	13.73
08	0.016	0.141	-2.001	19.585	0.327	0.000	0.54	18.11
09	0.020	0.110	-2.000	19.834	0.351	0.002	0.45	24.55
12	0.020	0.122	-2.005	18.477	0.382	-0.001	0.93	7.56
13	0.014	0.075	-2.005	19.498	0.142	0.000	-0.27	12.11
15	0.021	0.105	-2.000	19.901	0.332	0.000	0.69	15.93
17	0.023	0.135	-2.000	19.663	0.303	0.002	0.14	29.02

Table 3: PMB-NN identified lambda values and PMB-NN-R's performance

Participant	PM					
	λ_1	λ_2	λ_3	λ_4	λ_5	λ_6
01	0.030	0.060	-2.000	20.000	0.370	0.014
02	0.030	0.060	-2.000	20.000	0.100	0.024
03	0.014	0.060	-2.000	19.598	0.571	0.000
04	0.030	0.060	-2.000	20.000	0.341	0.000
05	0.030	0.060	-3.135	8.475	0.463	0.023
06	0.030	0.060	-2.000	20.000	0.258	-0.003
08	0.030	0.060	-2.000	20.000	0.346	-0.003
09	0.030	0.060	-2.000	20.000	0.346	0.001
12	0.030	0.060	-2.000	20.000	0.378	-0.002
13	0.010	0.150	-3.591	7.000	0.100	0.023
15	0.030	0.060	-2.000	20.000	0.224	0.024
17	0.030	0.060	-2.000	20.000	0.100	0.019

Table 4: PM identified lambda values

F Statistical summary and comparative analysis of estimation results across three models in different exercise conditions

The detailed activity-segmented R^2 and RMSE values for all models across both participants, and the one-tailed p-values for pairwise comparisons within each activity type between PMB-NN and FCNN, as well as PMB-NN and PM are provided in Table 5. P-values and Cohen’s d-values were derived from pairwise comparisons between PMB-NN and the respective models for identical metrics under each exercise condition.

Participant	Resting						Cycling						Running					
	PMB-NN			FCNN			PMB-NN			FCNN			PMB-NN			FCNN		
	R ²	RMSE	R ²	RMSE	R ²	RMSE	R ²	RMSE	R ²	RMSE	R ²	RMSE	R ²	RMSE	R ²	RMSE	R ²	RMSE
01	-0.75	5.02	0.02	3.76	-1.05	5.44	-8.46	5.24	-13.03	6.38	-4.68	4.06	0.17	4.40	0.79	2.23	-4.93	11.79
02	-0.98	4.11	-0.88	4.00	-3.27	6.03	-0.45	9.39	-0.70	10.20	-1.09	11.29	-9.46	22.26	-8.96	21.72	-35.17	41.40
03	-11.64	10.55	-1.93	5.07	-31.45	16.90	-9.18	3.80	-4.68	2.84	-122.49	13.24	-0.17	11.48	-3.04	21.31	0.69	5.95
04	-0.69	9.53	0.03	7.21	-1.52	11.63	0.29	5.75	-0.39	8.08	0.20	6.14	-68.35	17.65	-35.18	12.75	-162.52	27.11
05	-0.96	7.82	0.61	3.50	0.24	4.89	0.76	3.66	0.84	3.02	-1.42	11.70	-213.33	8.77	-195.36	8.39	-6176.94	47.06
06	-32.09	9.88	-7.77	5.08	-47.82	12.00	-1.48	5.73	-5.73	9.43	0.22	3.22	0.68	4.97	0.14	8.13	0.65	5.20
08	-40.20	10.51	-5.32	4.05	-37.42	9.98	0.68	4.09	0.91	2.11	-10.68	24.69	-25.69	6.21	-150.86	10.06	-200.90	11.60
09	-12.65	8.13	-5.97	4.51	-201.48	24.30	0.62	9.14	-0.13	15.68	-1.07	21.21	-719.48	38.77	-554.81	34.05	-147.94	17.63
12	0.26	7.03	0.80	3.68	0.60	5.18	0.93	3.31	0.87	4.65	0.84	5.19	-6.87	4.01	-3.67	3.09	-89.28	13.58
13	-12.38	9.64	-10.43	13.10	-4.71	9.26	-13.83	10.59	-13.21	9.59	-12.18	9.23	-20.67	17.60	-18.22	16.78	-68.30	31.87
15	-12.78	7.21	-22.96	9.57	-1.05	2.80	-1.98	4.70	0.35	2.19	-4.80	6.55	-5.19	28.26	-3.91	25.17	-4.33	26.22
17	-2.86	4.77	-5.67	6.73	-4.96	6.36	-12.27	8.22	-16.36	7.41	-427.88	36.85	-5.33	5.78	-2.59	4.16	-644.57	55.82
median	-6.31	8.83	-1.40	4.28	-17.36	10.80	-0.08	5.48	-0.55	7.23	-1.26	11.49	-17.57	10.13	-22.07	11.40	-91.56	14.71
max	-0.69	10.55	0.61	7.21	0.24	24.30	0.76	9.39	0.91	15.68	0.22	24.69	0.68	38.77	0.79	34.05	0.69	47.06
min	-40.20	4.11	-7.77	3.50	-201.48	4.89	-13.83	3.66	-16.36	2.11	-427.88	3.22	-719.48	4.40	-554.81	2.23	-6176.94	5.20
p value	—	—	0.092	0.064	0.519	0.424	—	—	0.470	0.519	0.129	0.034	—	—	0.151	0.470	0.064	0.077
d value	—	—	0.460	-0.607	-0.314	0.321	—	—	-0.214	0.256	-0.372	0.686	—	—	0.130	-0.047	-0.311	0.548

G Estimation results on participant 6 from PMB-NN-R and PM

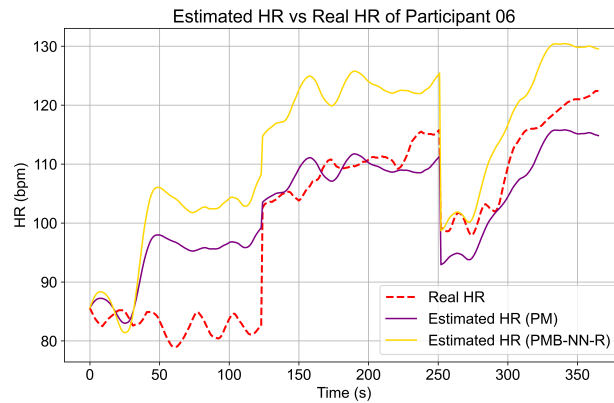


Figure 9: PMB-NN-R’s and PM’s HR estimation results of participant 6. The red dash curve in each plot represents the measured HR values, while the purple and gold solid curves represent the PM and PMB-NN-R estimated HR values, respectively.

H Data for participant 2

Figure 10 provided a sample of the same sudden increasing trend from sitting to standing among 5 participants’ data.

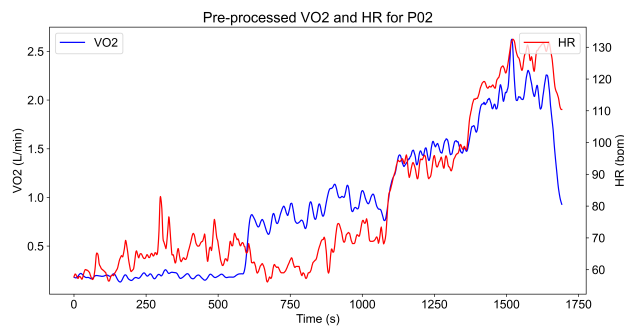


Figure 10: $\dot{V}O_2$ and HR data for participant 2 after preprocessing.

CRedit authorship contribution statement

Yaowen Zhang: Conceptualization, Formal Analysis, Methodology, Software, Validation, Visualization, Writing - Original Draft, Writing – review and editing. **Libera Fresiello:** Methodology, Supervision, Writing – review and editing. **Peter H. Veltink:** Supervision, Writing - Review and Editing. **Dirk W. Donker:** Supervision, Writing - Review and

Editing. **Ying Wang:** Conceptualization, Methodology, Supervision, Writing - Review and Editing.

Funding sources

Supported by the scholarship from China Scholarship Council (CSC).

Declaration of competing interest

The authors have no competing interests to declare.

References

- [1] C. Rogers, N. Bush. Heart failure: Pathophysiology, diagnosis, medical treatment guidelines, and nursing management. *The Nursing clinics of North America*, 50:787–99, 12 2015.
- [2] B. Steiner, et al. Challenges in heart failure care in four european countries: a comparative study. *European Journal of Public Health*, 33:448–454, 6 2023.
- [3] Y. Wang, et al. Early detection of heart failure with varying prediction windows by structured and unstructured data in electronic health records. pages 2530–2533. IEEE, 8 2015.
- [4] M. Hori, H. Okamoto. Heart rate as a target of treatment of chronic heart failure. *Journal of Cardiology*, 60:86–90, 8 2012.
- [5] M.T.L. Rovere, J.T. Bigger, F.I. Marcus, A. Mortara, P.J. Schwartz. Baroreflex sensitivity and heart-rate variability in prediction of total cardiac mortality after myocardial infarction. *The Lancet*, 351:478–484, 2 1998.
- [6] C.E. Pothier M.S. Lauer D.P. Vivekananthan, E.H. Blackstone. Heart rate recovery after exercise is apredictor of mortality, independent of the angiographic severity of coronary disease. *Journal of the American College of Cardiology*, 42:831–838, 9 2003.
- [7] N.J. Leeper, et al. Prognostic value of heart rate increase at onset of exercise testing. *Circulation*, 115:468–474, 1 2007.
- [8] C.E. Negrao, H.R. Middlekauff. Adaptations in autonomic function during exercise training in heart failure. *Heart Failure Reviews*, 13:51–60, 2 2008.
- [9] P. Lechat, et al. Heart rate and cardiac rhythm relationships with bisoprolol benefit in chronic heart failure in cibus ii trial. *Circulation*, 103:1428–1433, 3 2001.
- [10] S.J. Pocock, et al. Predictors of mortality and morbidity in patients with chronic heart failure. *European Heart Journal*, 27:65–75, 1 2006.

- [11] M. Jacobsen, T.A. Dembek, G. Kobbe, P.W. Gaidzik, L. Heinemann. Noninvasive continuous monitoring of vital signs with wearables: Fit for medical use? *Journal of Diabetes Science and Technology*, 15:34–43, 1 2021.
- [12] G. Quer, P. Gouda, M. Galarnyk, E.J. Topol, S.R. Steinhubl. Inter- and intraindividual variability in daily resting heart rate and its associations with age, sex, sleep, bmi, and time of year: Retrospective, longitudinal cohort study of 92,457 adults. *PLOS ONE*, 15:e0227709, 2 2020.
- [13] E. Magosso, M. Ursino. Cardiovascular response to dynamic aerobic exercise: A mathematical model. *Medical Biological Engineering Computing*, 40:660–674, 11 2002.
- [14] L. Fresiello, B. Meyns, A.D. Molfetta, G. Ferrari. A model of the cardiorespiratory response to aerobic exercise in healthy and heart failure conditions. *Frontiers in Physiology*, 7, 6 2016.
- [15] C.A. Sarmiento, A.M. Hernández, L.Y. Serna, M.Á. Mañanas. An integrated mathematical model of the cardiovascular and respiratory response to exercise: model-building and comparison with reported models. *American Journal of Physiology-Heart and Circulatory Physiology*, 320:H1235–H1260, 4 2021.
- [16] K. Bayoumy, M. Gaber, A. Elshafeey, et al. Smart wearable devices in cardiovascular care: where we are and how to move forward. *Nature Reviews Cardiology*, 18:581–599, 8 2021.
- [17] M. Yuchi, J. Jo. Heart rate prediction based on physical activity using feedforward neural network. pages 344–350. IEEE, 2008.
- [18] K. Mutijarsa, M. Ichwan, D.B. Utami. Heart rate prediction based on cycling cadence using feedforward neural network. pages 72–76. IEEE, 10 2016.
- [19] K. Hoffmann, J. Wiemeyer. Statistical models for predicting short-term hr responses to submaximal interval exercise, 2018.
- [20] D. Jang, B. Ko, S. Sunoo, S. Nam, H. Park, S. Bae. A preliminary study of a running speed based heart rate prediction during an incremental treadmill exercise. pages 5323–5326. IEEE, 8 2016.
- [21] F.M. Bennett, D.J. Christini, H. Ahmed, K. Lutchen, J.M. Hausdorff, N. Oriol. Time series modeling of heart rate dynamics. pages 273–276. IEEE Comput. Soc. Press.
- [22] M. Ludwig, A.M. Sundaram, M. Füller, A. Asteroth, E. Prassler. On modeling the cardiovascular system and predicting the human heart rate under strain. pages 106–117. SCITEPRESS - Science and Technology Publications, 2015.
- [23] M. Thoonen, P.H. Veltink, F.R. Halfwerk, R.W. van Delden, Y. Wang. A movement-artefact-free heart-rate prediction system. 12 2022.

- [24] J. Kubalík, E.Derner, R. Babuška. Toward physically plausible data-driven models: A novel neural network approach to symbolic regression. *IEEE Access*, 11:61481–61501, 2023.
- [25] G.E. Karniadakis, I.G. Kevrekidis, L. Lu, P. Perdikaris, S. Wang, L. Yang. Physics-informed machine learning, 6 2021.
- [26] S. Cai, Z. Wang, S. Wang, P. Perdikaris, G.E. Karniadakis. Physics-informed neural networks for heat transfer problems. *Journal of Heat Transfer*, 143, 6 2021.
- [27] M. Daneker, Z. Zhang, G.E. Karniadakis, L. Lu. Systems biology: Identifiability analysis and parameter identification via systems-biology-informed neural networks, 2023.
- [28] S. Gashi, C. Min, A. Montanari, S. Santini, F. Kawsar. A multidevice and multimodal dataset for human energy expenditure estimation using wearable devices. *Scientific Data*, 9:537, 9 2022.
- [29] M.M.H. Shandhi, et al. Estimation of instantaneous oxygen uptake during exercise and daily activities using a wearable cardio-electromechanical and environmental sensor. *IEEE Journal of Biomedical and Health Informatics*, 25:634–646, 3 2021.
- [30] M. Schmid, D. Rath, U. Diebold. Why and how savitzky-golay filters should be replaced. *ACS measurement science au*, 2:185–196, 4 2022.
- [31] A.E. Cetin, O.N. Gerek, Y. Yardimci. Equiripple fir filter design by the fft algorithm. *IEEE Signal Processing Magazine*, 14:60–64, 3 1997.
- [32] C. Scott. Misconceptions about aerobic and anaerobic energy expenditure. *Journal of the International Society of Sports Nutrition*, 2, 12 2005.
- [33] M.J. Sullivan, J.D. Knight, M.B. Higginbotham, F.R. Cobb. Relation between central and peripheral hemodynamics during exercise in patients with chronic heart failure. muscle blood flow is reduced with maintenance of arterial perfusion pressure. *Circulation*, 80:769–781, 10 1989.
- [34] F. Wilcoxon. Individual comparisons by ranking methods. *Biometrics Bulletin*, 1:80, 12 1945.
- [35] T.K. Koo, M.Y. Li. A guideline of selecting and reporting intraclass correlation coefficients for reliability research. *Journal of Chiropractic Medicine*, 15:155–163, 6 2016.
- [36] D.M. Cooper, C. Berry, N. Lamarra, K. Wasserman. Kinetics of oxygen uptake and heart rate at onset of exercise in children. *Journal of Applied Physiology*, 59:211–217, 7 1985.
- [37] H.A.M. Daanen, R.P. Lamberts, V.L. Kallen, A. Jin, N.L.U. Van Meeteren. A systematic review on heart-rate recovery to monitor changes in training status in athletes. *International Journal of Sports Physiology and Performance*, 7:251–260, 9 2012.

- [38] S. Rang, et al. Modelflow: a new method for noninvasive assessment of cardiac output in pregnant women. *American Journal of Obstetrics and Gynecology*, 196:235.e1–235.e8, 3 2007.
- [39] E.R. Valsangiacomo-Buechel et al. N. Kawel-Boehm, A. Maceira. Normal values for cardiovascular magnetic resonance in adults and children. *Journal of Cardiovascular Magnetic Resonance*, 17:29, 1 2015.
- [40] N. Naderi. Hemodynamic study, 2022.
- [41] T.A. Goers. *Washington University School of Medicine Department of Surgery; Klingensmith, Mary E; Li Ern Chen; Sean C Glasgow (2008). The Washington manual of surgery*. Philadelphia: Wolters Kluwer Health/Lippincott Williams & Wilkins, 2010.
- [42] J.E. Hall. *Guyton and Hall Textbook of Medical Physiology*. Elsevier, 14th edition, 2020. Accessed via PDFDrive.